

# An attempt to model the relationship between MMI attenuation and engineering ground-motion parameters using artificial neural networks and genetic algorithms

G-A. Tselentis<sup>1</sup> and L. Vladutu<sup>2</sup>

<sup>1</sup>Seismological Laboratory, University of Patras, RIO 265 04, Patras, Greece

<sup>2</sup>Mathematics Dept., Dublin City University, Dublin, Republic of Ireland

Received: 23 July 2010 – Accepted: 13 October 2010 – Published: 7 December 2010

**Abstract.** Complex application domains involve difficult pattern classification problems. This paper introduces a model of MMI attenuation and its dependence on engineering ground motion parameters based on artificial neural networks (ANNs) and genetic algorithms (GAs). The ultimate goal of this investigation is to evaluate the target-region applicability of ground-motion attenuation relations developed for a host region based on training an ANN using the seismic patterns of the host region. This ANN learning is based on supervised learning using existing data from past earthquakes. The combination of these two learning procedures (that is, GA and ANN) allows us to introduce a new method for pattern recognition in the context of seismological applications. The performance of this new GA-ANN regression method has been evaluated using a Greek seismological database with satisfactory results.

## 1 Introduction

A common problem encountered in engineering seismology involves the difficulty in assessing the damage potential of an earthquake based on the distribution of macroseismic intensity. This parameter is subject to interpretation due to the wide variation in geological conditions, the response of structures, uncertainty related to construction conditions before the earthquake, the type of construction, and population density. Obviously, a physically-based ground-related MMI is required for engineering purposes (Tselentis

and Danciu, 2008; Danciu and Tselentis, 2007). With the advent of instrumental seismology, the relationship between intensity and ground-motion parameters has become a topic of increasing interest.

Instrumental seismology offers the possibility to transform readily observed data (in this case, intensity) into widely-used parameters useful for engineering purposes (in this case, engineering ground-motion measures) and allows seismologists to evaluate historical earthquakes for which no instrumental data are available in order to assess seismic hazard and damages, correlate different intensity scales, and rapidly assess the severity of ground shaking.

Until recently, macroseismic intensity was related most frequently to peak ground acceleration (PGA) because of that parameter's importance for seismic-resistant design. This is due to the fact that the product of PGA and mass represents the inertial force loading structures (Krinitzsky and Chang, 1988). In recent years, research on earthquake damage prediction has concluded that other ground-motion characteristics such as duration, frequency, and energy content all contribute to structural damage.

Focusing either on regional or worldwide data, many empirical equations have been proposed to relate a seismic event's felt intensity with its peak ground velocity (PGV) (Panza et al., 1997; Wald et al., 1999; Wu et al., 2003; Kaka and Atkinson, 2004, 2007; Atkinson and Kaka, 2007), duration of ground motion (Trifunac and Westermo, 1977), response spectra (Kaka and Atkinson, 2007), Fourier spectra (Sokolov, 1998, 2002), cumulative absolute velocity (CAV) (Cabanac et al., 1997; Kostov, 2005), Arias intensity ( $I_a$ ) (Margottini et al., 1992), Housner's spectrum intensity, and JMA instrumental intensity (Karim and Yamazaki, 2002).



Correspondence to: G-A. Tselentis  
(tselenti@upatras.gr)

Recently, Tselentis and Danciu (2008) derived empirical regression equations for modified Mercalli intensity (MMI) and for various ground-motion parameters such as duration, CAV,  $I_a$ , characteristic intensity, Housner's spectrum intensity, and total elastic input energy index.

These relationships have been used to generate maps of estimated shaking intensities within a few minutes of the event based on recorded peak motions. These maps provide a rapid visualisation of the extent of expected damages following an earthquake and can be used for emergency response, loss estimation, and the release of public information through the media.

Another application of engineering ground-motion parameters involves the development of early warning systems. These systems are low-cost solutions aimed at reducing the seismic risk to vital facilities, such as nuclear power plants, pipelines, and high-speed trains. The ground-motion parameters and the damage potential threshold are essential for these systems.

The objective of the present investigation is to uncover the hidden, complex and often fuzzy relations between the engineering ground-motion parameters and macroseismic intensity and to express these relations in the form of input/output dependencies. The emergence of neural network technology (Haykin, 1999; Bishop, 1996) provides valuable insights for addressing the complicated problem of expression these relations. In this context, neural networks can be viewed as advanced mathematical models used to discover complex correlations between physical process variables from a set of perturbed observations.

## 2 Engineering seismological parameters

Because structure and equipment damage is measured according to its inelastic deformation, the potential for earthquake damage depends on the time duration of motion, the energy absorption capacity of the structure or equipment, the number of strain cycles, and the energy content of the earthquake. Therefore, for engineering purposes, parameters that incorporate in their definition these previously-mentioned characteristics are more reliable predictors of an earthquake's damage potential than parameters related solely to the amplitude of ground motion (such as peak ground acceleration, or PGA), which are often poor indicators of structural damage. The most commonly-used engineering ground-motion parameters in addition to PGA and PGV are Arias intensity ( $I_a$ ), acceleration response spectrum ( $S_a$ ), and cumulative absolute velocity (CAV).

$I_a$ , as defined by Arias (1970), is the total energy per unit weight stored by a set of undamped simple oscillators at the end of ground motion. The Arias intensity for ground motion

in the x-direction ( $I_{aX}$ ), is calculated as follows:

$$I_{aX} = \frac{2}{g} \int_0^t [a_X(t)]^2 dt, \quad (1)$$

where  $a_X(t)$  is the acceleration time history in the x direction, and  $t$  is the total duration of ground motion.

Spectrum acceleration ( $S_a$ ) is the most common-response spectral parameter and is related to spectrum velocity ( $S_v$ ) and spectrum displacement ( $S_d$ ) according to the following expression.

$$S_a = \frac{2\pi}{T} S_v = \omega S_v = \left(\frac{2\pi}{T}\right) S_d = \omega^2 S_d, \quad (2)$$

where  $T$  is the undamped natural period of a single-degree-of-freedom (SDOF) oscillator.

Cumulative absolute velocity (CAV) is defined as the integral of the absolute value of ground acceleration over the following seismic time-history record.

$$CAV = \int_0^t |a(t)| dt, \quad (3)$$

where  $|a(t)|$  is the absolute value of acceleration, and  $t$  is the total duration of ground motion.

## 3 Data set

The strong-motion records used for the present investigation were provided by the European Strong Motion Database (Ambraseys et al., 2004). More details on these data can be found in Danciu and Tselentis (2007). The macroseismic information was available in part from the digital database of the European strong-motion data; it was also separately estimated in part from the macroseismic data provided by the Geodynamic Institute of the National Observatory of Athens (Kalogeras et al., 2004). The general criterion of selecting the appropriate MMI value was to allocate at each station the nearest MMI values within an uncertainty of one unit to every station. If more than one MMI value was observed near the station location, at an equal distance from the station, the average of the values was used (Tselentis and Danciu, 2008).

Maps of the reported MMI values together with the strong-motion instrument locations were plotted to show reasonable confidence that the allocated MMI values are within one unit of the assigned value. This approach provides rapid visualisation of the macroseismic distribution in the area surrounding the recording stations and might be an efficient approach to assigning MMI values to minimise errors (Atkinson and Kaka, 2007).

At this preliminary stage of intensity ground-motion investigation, we decided not to disaggregate the soil effect because the soft soil subset comprises less than 30% of the total data set.

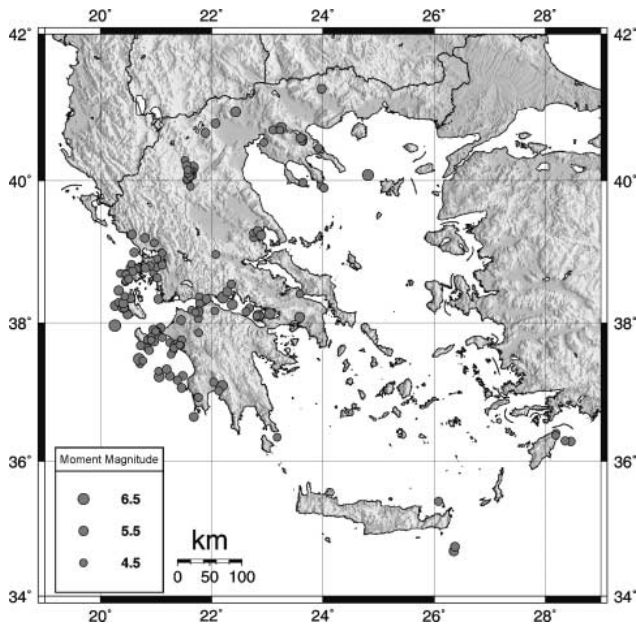


**Fig. 1.** Epicentral distribution of earthquakes used in the present analysis.

The final data set consists of 310 records from 151 earthquakes and is depicted in Fig. 1 and Table 1. Using the recorded strong-motion data for these earthquakes, for each horizontal component, we compute the previously mentioned engineering seismological parameters. The arithmetic average between the two horizontal components of the independent variables was used for the present investigation.

**4 Artificial neural networks**

An artificial neural network (ANN) is an information-processing paradigm inspired by the way biological nervous systems such as the brain process information. The most basic element of the human brain involves a specific type of cell that provides us with the ability to remember, think, and apply previous experiences to our every action. These cells are known as neurons. The power of the brain comes from the number of neurons and the multiple connections (or synapses) between them.

Figure 2 shows a simplified view of an ANN. It consists of a network of simple processing elements (that is, artificial neurons) that are organised in several layers, including an input layer that shows the number of neurons linked to the dimensionality of the input, one or several hidden layers, and an output layer. The hidden layer represents network inputs. When one presents the network with a form to be learned, the neurons simultaneously start a state of activity that causes a small modification of the synaptic forces between them. This is followed by a quantitative reconfiguration of all of the synapses: some of them become very strong, while others

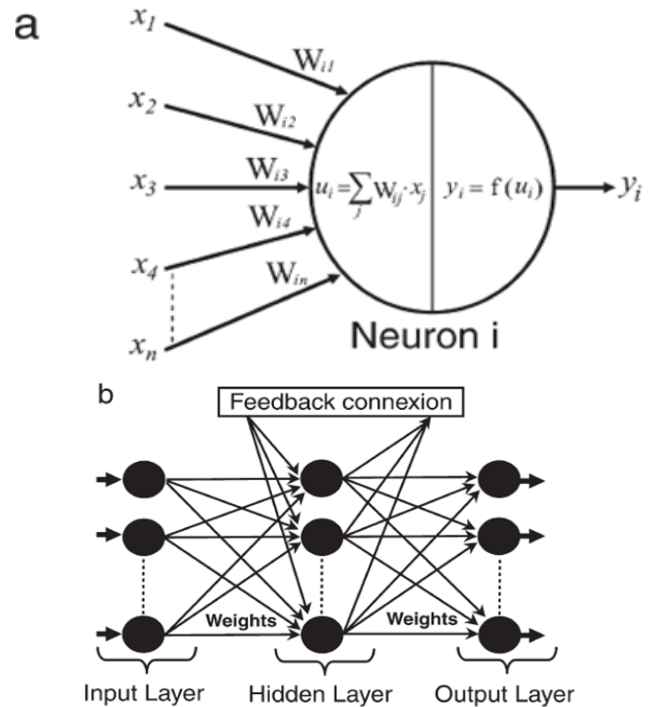


**Fig. 2.** General topology of a feed-forward ANN with one hidden layer.

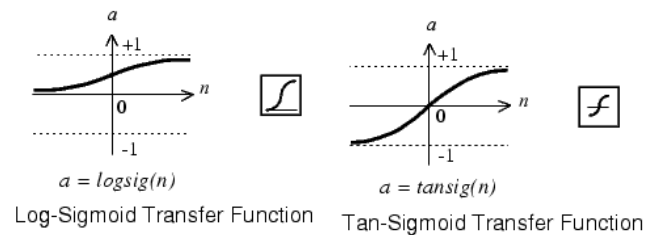


**Fig. 3.** Two classical nonlinear activation functions.

become weak. The learned form is not directly memorised at a precise place; it corresponds to a particular energy state of the network, which is a particular configuration of the activity of each neuron, across a very large set of possible configurations. This configuration is supported by the values of the synaptic forces.

Let  $Y_j^s$  represent the output of the  $j$ -th neuron at layer  $s$ ;  $W_{ij}^s$  is the weight connecting the  $i$ -th neuron in layer  $s$  to the  $j$ -th neuron at layer  $s-1$ . The neurons have their activation function characterised by a nonlinear function, such as the sigmoid function in Fig. 3. This function maps the output to its input and can be expressed by the following equation.

$$Y_j^s = f \left( b_j + \sum_{i=1}^R W_{ji}^s \cdot Y_i^{s-1} \right) \tag{4}$$

where  $b$  is the bias.

**Table 1.** Database of strong motion records used.

No	Earthquake Name	Date (dd-mm-yy)	Time	Latitude (°)	Longitude (°)	Moment Magnitude	Focal Depth (km)	Number of Records		
								B	C	D
1	Kefallinia Island	17/9/1972	14:07:12	38.245	20.263	5.6	1	0	0	2
2	Ionian	11/4/1973	15:52:12	38.78	20.55	5.8	7	1	0	0
3	Ionian	11/4/1973	16:11:36	38.76	20.65	4.9	15	1	0	0
4	Patras	29/1/1974	15:12:43	38.3	21.86	4.7	13	1	0	0
5	Amfissa	29/12/1977	16:52:59	38.55	22.35	5.1	10	1	0	0
6	Volvi	7/4/1978	22:23:28	40.7	23.106	5	6	1	0	0
7	Achaia	18/5/1978	00:18:49	38.3	21.79	4.5	26	1	0	0
8	Volvi	20/6/1978	20:03:22	40.729	23.254	6.2	6	3	1	0
9	Almiros (aftershock)	16/7/1980	00:06:58	39.21	22.76	5	12	0	1	0
10	Almiros (aftershock)	26/9/1980	04:19:21	39.27	22.75	4.8	5	0	1	0
11	Almiros (aftershock)	8/11/1980	09:15:59	39.3	22.83	5.2	5	0	1	0
12	Alkion	24/2/1981	20:53:39	38.099	22.842	6.6	10	2	0	0
13	Alkion	25/2/1981	02:35:53	38.135	23.05	6.3	8	1	0	0
14	Panagoula	25/5/1981	23:04:00	38.71	20.95	4.7	15	1	0	0
15	Levkas	27/5/1981	15:04:02	38.79	21.01	5.1	15	1	0	0
16	Preveza	3/10/1981	15:16:20	39.2	20.8	5.4	10	1	1	0
17	Paliambela	4/10/1981	08:33:32	38.91	21.02	4.7	10	1	0	0
18	Kefallinia Island	17/1/1983	12:41:31	37.96	20.26	6.9	5	1	1	0
19	Kefallinia (aftershock)	17/1/1983	15:53:57	38.13	20.49	5.2	11	0	1	0
20	Kefallinia (aftershock)	31/1/1983	15:27:02	38.12	20.49	5.4	4	0	1	0
21	Kyllini (foreshock)	20/2/1983	05:45:12	37.72	21.25	4.9	15	1	1	0
22	Etolia	16/3/1983	21:19:41	38.81	20.89	5.2	25	1	0	0
23	Kefallinia (aftershock)	23/3/1983	19:04:06	38.78	20.81	5.2	25	1	0	0
24	Kefallinia (aftershock)	23/3/1983	23:51:08	38.22	20.41	6.2	3	1	2	0
25	Off coast of Magion Oros peninsula	8/6/1983	15:43:53	40.08	24.81	6.6	22	0	1	2
26	Ierissos (foreshock)	14/6/1983	04:40:43	40.44	23.92	4.5	10	0	1	0
27	Ierissos	26/8/1983	12:52:09	40.45	23.92	5.1	12	0	1	2
28	Near southeast coast of Zakynthos Island	10/4/1984	10:15:12	37.64	20.85	5	6	0	1	0
29	Gulf of Corinth	17/8/1984	21:22:58	38.21	22.68	4.9	24	1	0	0
30	Arnissa	7/9/1984	18:57:12	40.66	21.89	5.2	5	0	1	1
31	Kranidia	25/10/1984	14:38:30	40.13	21.64	5.5	20	0	0	1
32	Kremidia (aftershock)	25/10/1984	09:49:15	36.93	21.76	5	11	0	0	2
33	Gulf of Amvrakikos	22/3/1985	20:38:39	38.99	21.11	4.5	6	0	0	1
34	Anchialos	30/4/1985	18:14:13	39.24	22.89	5.6	13	0	1	1
35	Gulf of Kiparissiakos	9/7/1985	10:20:51	37.24	21.25	5.4	10	0	0	1
36	Near coast of Preveza	31/8/1985	06:03:47	39	20.61	5.2	15	1	2	0
37	Drama	11/9/1985	23:30:43	41.26	23.98	5.2	18	0	2	2
38	Aghios Vasileios	18/2/1986	05:34:42	40.7	23.23	4.8	3	2	1	1
39	Skydra-Edessa	18/2/1986	14:34:04	40.79	22.07	5.3	10	0	1	1
40	Kalamata	13/9/1986	17:24:34	37.1	22.19	5.9	1	1	2	1
41	Kalamata (aftershock)	15/9/1986	11:41:28	37.03	22.13	4.9	12	0	3	1
42	Tsipiana	2/1/1987	05:35:36	37.86	21.77	4.5	20	0	1	0
43	Near northwest coast of Kefallinia Island	27/2/1987	23:34:52	38.46	20.33	5.7	5	1	2	0
44	Dodecanese	10/5/1987	09:27:02	36.29	28.46	5.3	6	0	1	1
45	Kounina	14/5/1987	06:29:11	38.17	22.06	4.6	9	0	1	0
46	Near northeast coast of Crete	2/9/1987	12:28:23	35.41	26.08	4.9	18	0	1	0
47	Kalamata (aftershock)	6/10/1987	14:50:12	37.24	21.48	5.3	30	1	1	1
48	Near southwest coast of Peloponnes	12/10/1987	22:51:14	36.65	21.68	5.2	18	0	0	1
49	Near northeast coast of Rodos Island	25/10/1987	13:02:00	36.3	28.36	5.1	10	0	0	1
50	Astakos	22/1/1988	06:18:55	38.64	21.02	5.1	10	1	0	0
51	Kefallinia Island	6/2/1988	10:35:25	38.32	20.43	4.8	10	0	1	0
52	Gulf of Corinth	4/3/1988	03:56:07	38.08	22.82	4.5	5	0	1	0
53	Ionian	24/4/1988	10:10:33	38.83	20.56	4.8	1	2	0	0
54	Gulf of Corinth	7/5/1988	20:34:52	38.1	22.86	4.9	10	1	1	0
55	Etolia	18/5/1988	05:17:42	38.35	20.47	5.3	26	0	2	1
56	Etolia	22/5/1988	03:44:15	38.35	20.54	5.4	15	2	2	0
57	Agrinio	3/8/1988	11:38:57	38.82	21.11	4.9	28	0	1	1

Table 1. Continued.

No	Earthquake Name	Date	Time	Latitude	Longitude	Moment Magnitude	Focal Depth	Number of Records		
								(dd-mm-yy)	(°)	(°)
58	Kyllini (foreshock)	22/9/1988	12:05:39	37.93	21.08	5.3	12	0	2	0
59	Kyllini (foreshock)	30/9/1988	13:02:54	37.69	21.33	4.7	5	1	1	0
60	Kyllini	16/10/1988	12:34:05	37.9	20.96	5.9	4	1	5	0
61	Trilofon	20/10/1988	14:00:59	40.53	22.94	4.8	20	3	1	1
62	Kyllini (aftershock)	22/10/1988	14:58:18	37.88	21.02	4.5	20	1	1	0
63	Kyllini (aftershock)	31/10/1988	02:59:51	37.85	21.01	4.8	18	1	1	0
64	Kyllini (aftershock)	27/11/1988	16:38:45	37.88	20.99	4.5	8	1	1	0
65	Patras	22/12/1988	09:56:50	38.37	21.78	4.9	10	1	2	0
66	Patras	15/5/1989	22:40:04	38.28	21.79	4.8	1	0	1	0
67	Patras	31/8/1989	21:29:31	38.06	21.76	4.8	23	1	1	0
68	Near southeast coast of Sithonia peninsula	9/3/1990	05:35:50	39.93	23.97	4.6	10	0	1	0
69	Aigion	17/5/1990	08:44:06	38.39	22.22	5.1	26	0	1	0
70	Near east coast of Zakynthos Island	20/5/1990	05:57:24	37.76	20.85	4.5	11	0	1	0
71	Zakynthos Island	24/5/1990	18:51:49	37.73	20.97	4.5	1	0	1	0
72	Near east coast of Zakynthos Island	24/5/1990	19:59:06	37.8	20.91	4.8	1	0	1	0
73	Plati	8/8/1990	00:35:07	37.15	22.04	4.9	10	0	2	0
74	Kefallinia Island	24/8/1990	12:54:41	38.24	20.43	4.5	9	0	1	0
75	Near southeast coast of Sithonia peninsula	9/9/1990	19:00:39	39.9	24.02	5	1	0	1	0
76	Kefallinia Island	4/10/1990	03:19:16	38.21	20.43	4.5	6	0	1	0
77	Griva	21/12/1990	06:57:43	40.95	22.43	6.1	1	1	2	3
78	Near southeast coast of Crete	19/3/1991	12:09:23	34.673	26.358	5.5	5	0	1	0
79	Near southeast coast of Crete	19/3/1991	21:29:27	34.74	26.376	5.2	9	0	1	0
80	Kefallinia Island	26/6/1991	11:43:32	38.34	21.044	5.3	4	0	3	0
81	Near north coast of Kefallinia Island	2/1/1992	09:05:18	38.29	20.325	4.5	9	0	1	0
82	Kefallinia Island	23/1/1992	04:24:17	38.28	20.41	5.6	3	0	3	0
83	Near northwest coast of Kefallinia Island	25/1/1992	12:23:23	38.38	20.44	4.5	10	0	1	0
84	Mataranga	30/5/1992	18:55:40	38.04	21.45	5.2	12	1	5	0
85	Tithorea	18/11/1992	21:10:41	38.26	22.37	5.9	15	1	3	0
86	Pyrgos (foreshock)	14/2/1993	10:17:45	37.71	21.38	4.5	4	1	0	0
87	Pyrgos (foreshock)	25/3/1993	05:44:09	37.61	21.31	4.5	5	1	0	0
88	Pyrgos (foreshock)	26/3/1993	11:45:16	37.68	21.44	4.9	3	3	3	0
89	Pyrgos (aftershock)	26/3/1993	12:49:13	37.69	21.42	4.7	10	1	1	0
90	Pyrgos (aftershock)	26/3/1993	12:26:30	37.55	21.27	4.5	19	1	0	0
91	Pyrgos (aftershock)	30/3/1993	19:08:57	37.64	21.32	4.5	10	0	1	0
92	Gulf of Corinth	2/4/1993	02:22:59	38.16	22.62	5	5	1	0	0
93	Off coast of Levkas Island	6/4/1993	03:24:27	38.7	20.45	4.8	1	0	1	0
94	Gulf of Corinth	11/4/1993	05:18:37	38.34	21.91	5.3	10	1	2	0
95	Pyrgos (aftershock)	29/4/1993	07:54:29	37.76	21.46	4.8	0	1	0	0
96	Near coast of Filiatra	3/5/1993	06:55:06	37.07	21.46	5.2	1	0	1	3
97	Mouzakaiika	13/6/1993	23:26:40	39.25	20.57	5.3	5	2	3	0
98	Patras	14/7/1993	12:31:50	38.16	21.76	5.6	13	3	4	0
99	Patras (aftershock)	14/7/1993	12:39:13	38.18	21.64	4.6	10	1	2	0
100	Patras (aftershock)	14/7/1993	12:54:07	38.15	21.71	4.6	10	1	0	0
101	Pyrgos (aftershock)	7/10/1993	20:26:04	37.79	21.11	4.8	10	0	1	0
102	Near southwest coast of Levkas Island	9/10/1993	13:33:20	38.58	20.45	4.6	6	0	1	0
103	Off coast of Levkas Island	12/1/1994	07:32:57	38.702	20.359	4.6	7	0	1	0
104	Ionian	14/1/1994	06:07:48	37.61	20.88	4.9	10	0	1	0
105	Komilion	25/2/1994	02:30:50	38.73	20.58	5.4	5	2	3	0
106	Ionian	27/2/1994	22:34:52	38.69	20.46	4.8	10	2	1	0
107	Near southwest coast of Levkas Island	15/3/1994	22:41:04	38.602	20.459	4.5	0	0	1	0
108	Arta	14/4/1994	23:01:34	39.132	20.968	4.5	1	0	1	0
109	Levkas Island	18/7/1994	15:44:18	38.626	20.507	4.9	3	0	1	0
110	Paliouri	4/10/1994	19:46:21	39.976	23.643	5.1	10	0	1	0
111	Zakynthos Island	17/10/1994	09:02:17	37.756	20.912	4.6	14	0	1	0
112	Arnaia (foreshock)	5/3/1995	15:39:56	40.541	23.642	4.7	8	0	1	1
113	Arnaia (foreshock)	5/3/1995	21:36:54	40.58	23.65	4.6	8	0	1	2
114	Arnaia (foreshock)	4/4/1995	17:10:10	40.545	23.625	4.6	9	0	1	1
115	Arnaia	5/4/1995	0:34:11	40.59	23.6	5.3	14	0	2	2

Table 1. Continued.

No	Earthquake Name	Date (dd-mm-yy)	Time	Latitude (°)	Longitude (°)	Moment Magnitude	Focal Depth (km)	Number of Records		
								B	C	D
116	Kozani	13/5/1995	8:47:15	40.183	21.66	6.5	14	0	3	5
117	Kozani (aftershock)	13/5/1995	11:43:31	40.1	21.6	5.2	10	0	0	1
118	Kozani (aftershock)	13/5/1995	18:06:01	40.28	21.52	4.6	29	0	0	1
119	Kozani (aftershock)	14/5/1995	14:46:57	40.13	21.66	4.5	0	0	1	0
120	Kozani (aftershock)	15/5/1995	04:13:57	40.08	21.65	5.2	9	0	3	1
121	Kozani (aftershock)	16/5/1995	23:00:42	40.02	21.56	4.7	0	0	1	0
122	Kozani (aftershock)	16/5/1995	23:57:28	40.09	21.62	4.9	0	0	2	0
123	Kozani (aftershock)	16/5/1995	04:37:28	40.01	21.58	4.8	9	0	1	0
124	Kozani (aftershock)	17/5/1995	04:14:25	40.046	21.58	5.3	10	0	3	1
125	Kozani (aftershock)	17/5/1995	09:45:07	40.01	21.56	5	0	0	2	0
126	Kozani (aftershock)	18/5/1995	06:22:55	40.03	21.56	4.6	0	0	1	0
127	Kozani (aftershock)	19/5/1995	06:48:49	40.09	21.6	5.2	7	0	4	0
128	Kozani (aftershock)	19/5/1995	07:36:19	40.06	21.61	4.8	0	0	1	0
129	Kozani (aftershock)	6/6/1995	04:36:00	40.14	21.61	4.8	0	0	4	1
130	Aigion	15/6/1995	00:15:51	38.362	22.2	6.5	10	1	8	1
131	Kozani (aftershock)	17/7/1995	23:18:15	40.21	21.55	5.2	22	0	1	1
132	Kozani (aftershock)	18/7/1995	07:42:54	40.101	21.575	4.7	10	0	1	0
133	Aigion (aftershock)	13/8/1995	05:17:29	38.101	22.81	4.5	8	0	1	0
134	Kozani (aftershock)	6/11/1995	18:51:48	39.92	21.62	4.8	13	0	5	1
135	East of Kithira Island	29/6/1996	01:09:03	36.351	23.179	4.5	6	0	0	1
136	Pyrgos	8/11/1996	11:43:45	37.684	21.425	4.7	0	0	1	0
137	Zakynthos Island	16/2/1997	11:03:19	37.676	20.723	4.9	8	0	1	0
138	Strofades (foreshock)	26/4/1997	22:18:34	37.181	21.385	5	7	0	0	1
139	Strofades (foreshock)	29/4/1997	23:52:17	37.416	20.713	4.5	2	0	1	0
140	South of Vathi	11/5/1997	10:27:56	38.412	23.588	4.6	30	0	3	0
141	Itea	11/5/1997	21:10:28	38.44	22.28	5.6	24	0	3	1
142	South of Rhodes	17/7/1997	13:21:01	36.412	28.192	4.5	5	0	1	1
143	South of Rhodes	18/7/1997	1:45:23	36.38	28.188	4.6	14	0	1	1
144	Varis	22/8/1997	03:17:47	40.148	21.572	4.5	23	0	0	1
145	Northwest of Makrakomi	21/10/1997	17:57:47	38.971	22.073	4.7	14	0	0	1
146	Strofades	18/11/1997	13:07:41	37.482	20.692	6.6	10	2	6	2
147	Strofades (aftershock)	18/11/1997	13:13:46	37.229	21.057	6	10	1	3	2
148	Strofades (aftershock)	18/11/1997	15:23:35	37.334	21.191	5.3	30	1	1	1
149	Strofades (aftershock)	18/11/1997	13:44:05	37.309	21.047	4.8	10	0	1	0
150	Strofades (aftershock)	19/11/1997	00:33:07	37.458	20.764	4.8	10	0	1	0
151	Ano Liosia	9/7/1999	11:56:51	38.08	23.58	6	17	2	7	0
Total no. of records								75	197	63

This relation, by establishing the input of the first layer of the network, allows us to gradually calculate the value of the global output of the network, thus ensuring its forward propagation. When one compares this output with the desired output, one can calculate the error function, generally given by

$$e = \frac{1}{2} (Y - \bar{Y})^2 \quad (5)$$

where  $Y$  is the desired output, and  $(\bar{Y})$  is the obtained output. The direction in which the weights are updated is given by the negative of the gradient of  $(e)$  with respect to every element of the weight. This process consists in minimising  $(e)$  by a gradient descent. Thus, we try to modify the synaptic weights to reduce  $(e)$ . This is carried out using the following relation.

$$\Delta w_{ij}^s = -\mu \left( e_j^s Y_i^{s-1} \right)_n + \left( \Delta w_{ji}^s \right)_{n-1} \quad (6)$$

where  $\mu$  is the learning rate parameter, which usually takes values between 0 and 0.5. The quantity  $e_j^s$  is the locale of the error of the  $j$ -th neuron in the  $s$  layer. Weights and bias terms are first initialised at random values. In general, there are no strict rules for determining the network configuration for optimum training and prediction.

One representation of the ANN used in the present investigation is shown in Fig. 4, which includes the most commonly-used engineering seismological ground-motion parameters as inputs.

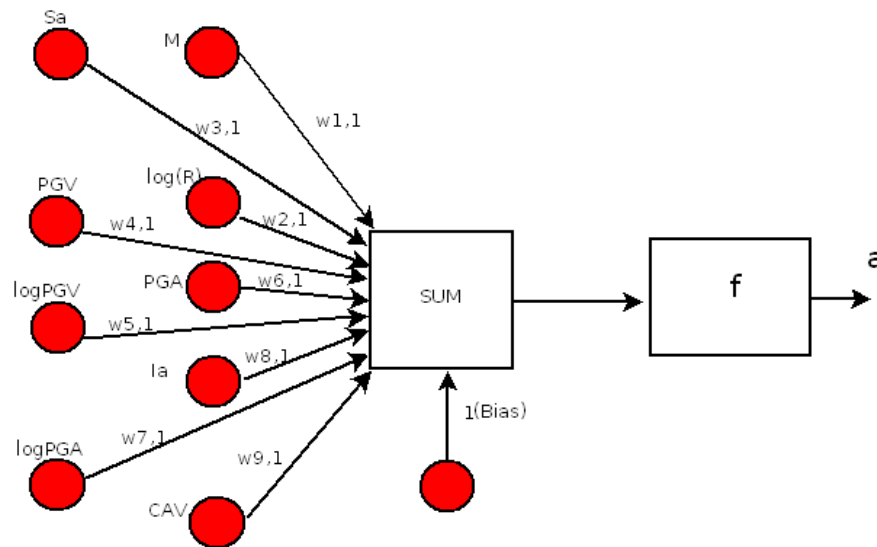


Fig. 4. Topology of the feed-forward k-NN-type ANN used in the present study.

## 5 Data processing

We consider automatic MMI assessment based on ground-motion parameters as part of a larger category of problems encountered in pattern recognition (Poggio and Girosi, 1990). In the present investigation, we consider the following four phases: (1) feature extraction, (2) classification, (3) pre-processing and optimisation and (4) regression.

### 5.1 Feature extraction

During this phase, we combined the enhanced selection capacities offered by GA with the performance of an ANN as a classifier. At first, we used all nine commonly-used input parameters that characterise earthquake ground motion at a site corresponding to an MMI value. These measures include  $M$ ,  $\log(R)$ , PGV,  $\log(\text{PGV})$ ,  $S_a$ , PGA,  $\log(\text{PGA})$ ,  $I_a$  and CAV (Fig. 4). During this procedure, we use 9-bit string ( $S$ ) quantification with binary field-values as follows.

$$S = [M, \log R, S_a, \text{PGV}, \log \text{PGV}, \text{PGA}, \log \text{PGA}, I_a, \text{CAV}] \quad (7)$$

For example, the three-parameter string  $[\log R, I_a, \text{CAV}]$  is represented as the string **01000011**. A genetic algorithm was used to generate populations of strings out of the 512 possible combinations from **00000000** to **11111111**. The total number of available strings (that is, the equivalent of chromosomes) at a certain time (i.e., after the Max-No-Generations), which is known as the genome, was evaluated by an ANN implemented as a k-nearest neighbour (k-NN). This was achieved by comparing the corresponding MMI (that is, the outputs) with the selected inputs out of the nine possible inputs represented by the strings generated by the

genetic algorithm. In our implementation, we have allowed a population size of 20, where the population size indicates the maximum number of chromosomes (or strings) allowed in a generation.

### 5.2 Classification

The second phase, which deals with classification, is implemented using a k-NN-type neural network. The k-nearest neighbours (k-NN) algorithm is a method for classifying objects based on the closest training examples in the feature space. The k-NN algorithm is a type of instance-based learning, or lazy learning, where the function is only approximated locally, and all computation is deferred until classification.

In the machine-learning community, *Instance-Based Learning* (IBL) (Aha et al., 1991), also known as memory-based learning, is a family of learning algorithms that, instead of performing explicit generalisations, compares new instances with instances that have been observed during training. It is called instance-based because it constructs hypotheses directly from the training instances themselves. A direct consequence of this approach is that the complexity of the problem grows with the amount of data available for training and testing.

Of the data set of 310 values, some data points were left for testing, while most were considered for training. We have used a GA-ANN with IBL approach in order to avoid data changes produced by normalisation techniques. The Euclidean metric is used to assess distances between the training and testing epochs.

In our approach, we used one of the simplest examples of IBL, namely, k-NN classifier and its Java implementation based on the Weka-toolbox (Witten and Frank, 2005).

The k-NN classifier is amongst the simplest machine-learning algorithms. In our case, it selects the optimal combination of the nine inputs (see Eq. 7). An object is an instance out of the 310 data values given in the features space; it is a five-parameter string consisting of  $[M, \log(R), \text{PGA}, I_a, \text{CAV}]$ . It is classified by a majority vote of its neighbours, with the object being assigned to the class most common among its k-nearest neighbours.

### 5.3 Pre-processing and optimisation

In the previous two phases, we considered all inputs as they were, but for processing purposes, we converted all inputs into integers by multiplying them by powers of 10 (Hårdle et al., 1995; Mierswa et al., 2006).

Candidate solutions to the optimisation problem act like individuals in a population, and a fitness function determines the environment within which these solutions “live” (e.g., a cost function). Genetic algorithms are a particular class of evolutionary algorithms (EA) (Fonseca and Fleming, 1995) that use techniques inspired by evolutionary biology such as inheritance, mutation, selection, and crossover (or recombination).

In other words, a GA quantifies information (namely, the parameters of the k-NN classifier) in the form of strings (that is, the chromosomes), and through the EA, only the fittest chromosomes survive over the generations of the evolution. Therefore, an important parameter for the proposed GA-ANN method is Max-No-Gener, which allows the GA algorithm to evolve to achieve the optimal solution. In our case, there are several parameters that have to be modified (or fine-tuned) to achieve optimal behaviour according to ANN. These include the number of hidden layers and the number of neurons in each hidden layer.

After finding the optimal Max-No-Gener parameter, we determined  $k$  and the selection scheme (or the size of the tournament).  $k$  was found by a trial-and-error procedure to have a value of 2. One advantage of the selection mechanism of a GA (Tobias and Lothar, 1995) is the independence of the representation of the individuals. Only the fitness values of individuals are taken into account.

A fitness function is a particular type of objective function that prescribes the optimality of a solution (or chromosome) in a genetic algorithm so that a particular chromosome may be ranked among all other chromosomes from the genome. Chromosomes which are found to be “more optimal” are allowed to breed. That is, further binary combinations will be created by the GA on the “skeleton” of these “more optimal” chromosomes. Data sets can then be mixed using any of several available techniques, thus producing a new generation of chromosomes. This mix in our case can be represented by taking the first four digits from one “optimal” string and the last five digits from another “more optimal” one, thereby creating a new chromosome (9-digit string)

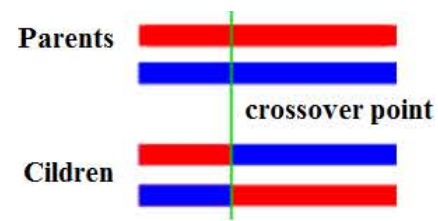


Fig. 5. One-point crossover.

that can possibly perform better under k-NN classification. This simplifies the analysis of the selection methods and allows a comparison that can be used for all kinds of genetic algorithms.

One of the frequently-used selection schemes is tournament selection. In this scheme, we run a tournament among a few individuals chosen at random from the population (i.e., from the genome) and select the one with the best fitness for crossover as the winner, adjusted by variances in tournament size. In genetic algorithm theory, the crossover is the genetic operator used to modify the programming of a chromosome or a group of chromosomes from one generation to the next. It is analogous to natural reproduction and biological crossover upon which the simplified GA theory for computational intelligence was built.

First, a single crossover point on the strings of both parent organisms is selected while avoiding extreme points. All data beyond that point in either organism string are swapped between the two organism strings. The resulting organisms are the children (or offspring), as shown in Fig. 5.

If the tournament size is larger (chromosomes for which the objective function, i.e., the error has a higher value), weak individuals have a smaller chance of being selected for breeding, crossover, and perpetuation in the next generations. Performance was quantified by RMS criteria and the squared error. A flow chart describing all of the above operations is presented in Fig. 6.

To validate the performance of the above-mentioned GA-ANN selection schemes, we selected a validation scheme based on regression performance. The results for the selection of the first optimal parameter from those described above (that is, Max-No-Gener) are presented in Table 2. From this table, we note the following cases.

Supposing that Max-No-Gener = 75 and that we obtained  $S_1$  as the fittest string, where  $S_1$  is given by the GA+k-NN algorithm and corresponds to the combination  $[M, \log(R), \log(\text{PGV}), I_a, \text{CAV}]$ . This is represented as **110010011**. The fittest chromosome is considered the one for which the objective function has an extreme value. In our case, the objective function is the squared error of the k-NN type of ANN, and so the objective function must have a minimum value.

**Table 2.** The parameters retained by the GA-ANN selection algorithm and corresponding regression performance (columns 2 and 3).

Max-No-Gener.	Sq error	RMS error	root_relative_squared_error	The retained parameters
75	0.329 ± 0.170	0.553 ± 0.152	0.608 ± 0.178	$S_1 = [M, \log R, \log PGV, I_a, CAV]$
80	<b>0.311 ± 0.154</b>	<b>0.456 ± 0.169</b>	<b>0.593 ± 0.195</b>	$S_2 = [M, \log R, PGA, I_a, CAV]$
90	0.339 ± 0.231	0.548 ± 0.196	0.618 ± 0.189	$S_3 = [\log R, I_a, CAV]$
94	0.324 ± 0.194	0.571 ± 0.176	0.608 ± 0.194	$S_4 = [M, \log R, S_a, \log PGV, PGA, I_a, CAV]$

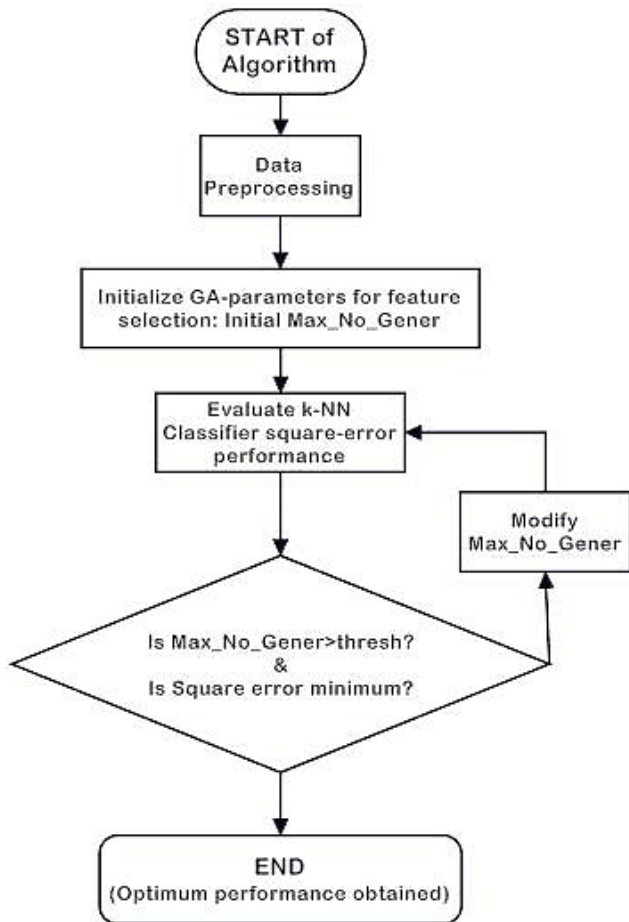


**Fig. 6.** Flowchart showing the sequences of feature-selection and classification.

If we consider the case with Max-No-Gener = 80 with  $S_2$  as the fittest string, this corresponds to the combination  $[M, \log(R), PGA, I_a, CAV]$  and is represented as **110001011**. In this situation,  $S_2$  is retained as having the best fitness because the output of the k-NN classifier for  $S_1$  is given by the squared error  $0.329 \pm 0.170$  and for  $S_2$  is given by of the squared error of  $0.311 \pm 0.154$ . In other words, both the error and its standard deviation are lower than in the case of  $S_1$ .

Setting Max-No-Gener higher than optimally at 90,  $S_3$  then corresponds to the combination  $[\log R, I_a, CAV]$  and is represented as **010000011**; this solution is rejected due to a worse regression performance (that is, a higher RMS error). The solution with Max-No-Gener = 94 and string  $S_4$  corresponding to the combination  $[M, \log R, S_a, PGV, \log PGV, PGA, \log PGA, I_a, CAV]$  and represented by **111111111** is also rejected because it accepted almost all of the input parameters and is a trivial solution.

Finally, an underdetermined solution, which results if values of Max-No-Gener are in the range of 25 to 70, is rejected because GAs require a minimum number of generations to obtain optimal fitness among all available individuals.

Judging from the above, an optimal value of Max-No-Gener = 80 with a minimum RMS was selected. In this case, the optimal selected input parameters are  $M, \log R, PGA, I_a,$  and  $CAV$ . These are the parameters used to express MMI throughout the regression process.

### 5.4 Regression

In a case in which the existing data are not sufficient for analysis because we must use part of the data for validation and test sets, it is common to use a cross-validation or rotation estimation method (Kohavi, 1995). This is a technique for assessing how the results of a statistical analysis will generalise to an independent data set. It is mainly used in applications in which the goal is prediction, particularly when one wants to estimate how accurately a predictive model will perform in practice. Cross-validation involves partitioning a portion of the data into complementary subsets, performing analysis on one subset called the training set, and validating the analysis on the other subset, which is called the validation or testing set. For relatively large datasets, a higher cross-validation is usually used (25 in our case).

Next, the selected optimal input parameters  $[M, \log R, PGA, I_a,$  and  $CAV]$  are considered as  $X$  multivariate inputs, and the response variable  $Y$  is understood to indicate MMI. To calculate the coefficients that link  $Y$  to the five-dimensional  $X$  variable, we used the linear

**Table 3.** The parameters for linear regression obtained by the program XploRe for the input data selected by the proposed GA-ANN method.

PARAMETERS	Beta	SE	StandB	t-test	p-value
b[0,]	8.8236	4.0481	0.0000	1.439	0.1513
b[1,]	0.4173	0.9553	0.2733	0.437	0.6625
b[2,]	-7.9601	12.2908	-0.4084	-0.648	0.5177
b[3,]	0.3801	0.4533	0.1499	0.839	0.4024
b[4,]	1.1046	0.5022	0.7718	2.200	0.0286
b[5,]	-0.5508	0.5965	-0.2046	-0.923	0.3566

**Table 4.** The statistical parameters obtained for the linear regression using the ANOVA test.

ANOVA	SS	df	MSS	F-test	p-value
Regression	155.893	5	31.179	67.556	0.0000
Residuals	140.30	4 304	0.462		
Total Variation	296.197	309	0.959		
Multiple $R$	= 0.72548				
$R^2$	= 0.52632				
Adjusted $R^2$	= 0.51853				
Standard Error	= 0.67936				

regression approach described by the following equation (Härdle et al., 1995).

$$Y = b_0 + \sum_{i=1}^5 b_i * X_i \quad (8)$$

where  $b_0$  is the intercept, and  $b_1, \dots, b_5$  are the coefficients for the ground parameters.

The obtained  $b$  values are presented in Table 3, and the results of the ANOVA statistical test are shown in Table 4. Accordingly, the relation that describes MMI as a function of  $[M, \log R, PGA, I_a, CAV]$  is as follows.

$$\begin{aligned} \text{MMI} = & 8.824 + 0.417M - 7.960 \log R + 0.380PGA \\ & + 1.105I_a - 0.551CAV \end{aligned} \quad (9)$$

Figure 7 shows the time series corresponding to the original data and the results of the regression analysis. For the GA-ANN selection scheme, we used a Java-based implementation built around the Weka (the IBk lazy learner) data-mining system (Witten and Frank, 2005).

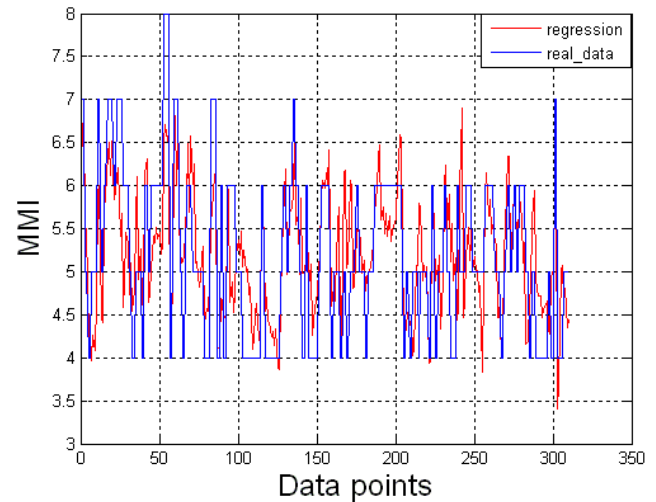


**Fig. 7.** Output of the regression algorithm (in red) and the original MMI data (in blue) for the 310 considered data points.

## 6 Conclusions

In this research, we presented a new approach based on ANN and GA to model the relationship between MMI attenuation and engineering ground motion parameters. The performance of this new regression approach has been tested using a Greek strong motion database with satisfactory results.

We note that not all of the features selected in the GA-ANN approach have the same influence on MMI attenuation. An approach based on evolutionary algorithms can be useful in weighting the importance of those features. Additionally, a new type of neural network (namely, an evolutionary neural network) can be used to replace the classical k-NN used in the current paper. If we implement an expert system, we can derive a real-time signal-processing system, which can be used for near real-time damage assessment and shake map construction.

*Acknowledgements.* We are grateful to Laurentin Danciu for his most useful comments. The help of M. E. Condakis and 2 anonymous reviewers is greatly appreciated.

Edited by: M. E. Contadakis

Reviewed by: two anonymous referees

## References

- Ambraseys, N., Smit, P., Douglas, J., Margaris, B., Sigbjornsson, R., Olafsson, S., Suhadolc, P., and Costa, G.: Internet-site for European strong-motion data, *Boll. Geofis. Teor. Appl.* 45(3), 113–129, 2004.
- Aha, D. W.: *Instance-based Learning, Machine Learning*, Kluwer Academic Publishers, 6, 36–77, 1991.

- Arias, A.: A measure of earthquake intensity, Cambridge, MA, 1970.
- Atkinson, G. M. and Kaka, S. I.: Relationship between felt intensity and instrumental ground motion in the central United States and California, *B. Seismol. Soc. Am.*, 97(2), 497–510, 2007.
- Bishop, C. M.: *Neural Networks for Pattern Recognition*, Oxford University Press, UK, 1996.
- Cabanas, L., Benito, B., and Herraiz, M.: An approach to the measurement of the potential structural damage of earthquake ground motions, *Earthq. Eng. Struct. D.*, 26, 79–92, 1997.
- Danciu, L. and Tselentis, G-A.: Engineering ground motion parameters attenuation relationships for Greece, *B. Seismol. Soc. Am.*, 97(1B), 162–183, 2007.
- Fonseca, C. M. and Fleming, P. J.: Multi-objective genetic algorithms made easy: Selection, sharing and mating restriction, in: *Proceedings of the first international conference on generic algorithms in engineering systems: Innovations and applications*, Sheffield, UK, 45–52, 1995.
- Fujinawa, Y., Matsumoto, T., and Takahashi, K.: Method for estimating origin time, hypocentral distance and scale based on electric field observation, and apparatus for prediction, Patent No. US 6,885,945 B2, 2005.
- Härdle, W.: *Applied Nonparametric Regression*, Humboldt-Universität zu Berlin Wirtschaftswissenschaftliche Fakultät Institut für Statistik und Ökonometrie, 1994.
- Härdle, W., Klinkle, S., and Turlach, B.: *XploRe – an Interactive Statistical Computing, Environment*, Springer, Heidelberg, 1995.
- Haykin, S.: *Neural Networks*, 2nd edn., MacMillan College Publishing Company, 1999.
- Kaka, S. I. and Atkinson, G. M.: Relationships between felt intensity and instrumental ground motion in the central United States and California, *B. Seismol. Soc. Am.*, 97(2), 497–510, 2004.
- Kalogeras, I. S., Marketos, G., and Theodoridis, Y.: A tool for collecting, verifying, and mining macroseismic data, *B. Geol. Soc. Greece*, XXXVI, 2004.
- Karim, K. R. and R. Yamazaki, R.: Correlation of JMA instrumental seismic intensity with strong motion parameters, *Earthq. Eng. Struct. D.*, 31(5), 1191–1212, 2002.
- Kohavi, R.: A study of cross-validation and bootstrap for accuracy estimation and model selection, *Proceedings of the Fourteenth International Joint Conference on Artificial Intelligence*, (Morgan Kaufmann, San Mateo), 2(12), 1137–1143, 1995.
- Koliopoulos, P. K., Margaritis, B. N., and Klimis, N. S.: Duration and energy characteristics of Greek strong motion records, *J. Earthq. Eng.*, 391–417, 1998.
- Kostov, M. K.: Site specific estimation of cumulative absolute velocity, 18th International Conference on Structural Mechanics in Reactor Technology, Beijing, China, 2005.
- Krinitzky, E. L. and Chang, F. K.: Intensity-related earthquake ground motion, *Bull. Int. Assoc. Eng. Geol.* 4, 425–435, 1988.
- Margottini, C., Molin, D., and Serva, L.: Intensity versus ground motion: a new approach using Italian data, *Eng. Geol.*, 33, 45–58, 1992.
- Mierswa, I., Wurst, M., Klinkenberg, R., Scholz, M., and Euler, T.: YALE: Rapid prototyping for Complex Data Mining Tasks, in *Proceedings of the 12th ACM SIGKDD International Conference on Data Mining and Knowledge Discovery*, (KDD-06), 2006.
- Panza, G. F., Cazzaro, R., and Vaccari, F.: Correlation between macroseismic intensities and seismic ground motion parameters, *Ann. Geofis.*, 40(5), 1371–1382, 1997.
- Poggio, T. and Girosi, F.: Regularization algorithms for learning that are equivalent to multilayer perceptrons, *Science*, 247, 978–982, 1990.
- Sokolov, Y. V.: Spectral parameters of the ground motions in Caucasian seismogenic zones, *B. Seismol. Soc. Am.*, 88(6), 1438–1444, 1998.
- Skolov, Y. V.: Seismic Intensity and Fourier Acceleration Spectra: Revised Relationship, *Earthq. Spectra*, 18(1), 161–187, 2002.
- Tobias, B. and Lothar, T.: A comparison of selection schemes used in evolutionary algorithms, *Evol. Comput.*, 4(4), 361–394, 1995.
- Trifunac, M. D. and Westermo, B.: A note on the correlation of frequency-dependent duration of strong earthquake ground motion with the modified Mercalli intensity and the geologic conditions at the recording stations, *B. Seismol. Soc. Am.*, 67(3), 917–927, 1977.
- Tselentis, G-A. and Danciu, L.: Empirical relationships between MMI and engineering ground motion parameters in Greece, *B. Seimol. Soc. Am.*, 98(4), 1863–1875, 2008.
- Witten, I. H. and Frank, E.: *Data Mining – Practical Machine Learning Tools and Techniques*, Elsevier, 2005.
- Wald, D. J., Quitoriano, V., Heaton, T. H., and Kanamori, H.: Relationships between peak ground acceleration, peak ground velocity, and modified mercalli intensity in California, *Earthq. Spectra*, 15(3), 557–564, 1999.
- Wu, Y. M., Teng, T. I., Shin, T. C., and Hsiao, N. C.: Relationship between peak ground acceleration, peak ground velocity and intensity in Taiwan, *B. Seismol. Soc. Am.*, 93, 386–396, 2003.